

A practical set of miniaturized instruments for vertical profiling of aerosol physical properties

Hagen Telg, Daniel M. Murphy, Timothy S. Bates, James E. Johnson, Patricia K. Quinn, Fabio Giardi, and Ru-Shan Gao

QUERY SHEET

This page lists questions we have about your paper. The numbers displayed at left can be found in the text of the paper for reference. In addition, please review your paper as a whole for correctness.

- Q1.** Au: Please provide the department name in affiliation “e.”
- Q2.** Au: Please provide the last page number in reference “Kassianov et al. (2015).”
- Q3.** Au: Please provide the last page number in reference “Twohy et al. (2009).”

TABLE OF CONTENTS LISTING

The table of contents for the journal will list your paper exactly as it appears below:

A practical set of miniaturized instruments for vertical profiling of aerosol physical properties

Hagen Telg, Daniel M. Murphy, Timothy S. Bates, James E. Johnson, Patricia K. Quinn, Fabio Giardi, and Ru-Shan Gao



A practical set of miniaturized instruments for vertical profiling of aerosol physical properties

Hagen Telg^{a,b}, Daniel M. Murphy^a, Timothy S. Bates^{c,d}, James E. Johnson^{c,d}, Patricia K. Quinn^c, Fabio Giardi^e, and Ru-Shan Gao^a

- 5 ^aNOAA Earth System Research Laboratory (ESRL), Boulder, Colorado, USA; ^bCooperative Institute for Research in Environmental Sciences (CIRES), University of Colorado, Boulder, Colorado, USA; ^cNOAA Pacific Marine Environmental Laboratory, Seattle, Washington, USA; ^dJoint Institute for the Study of the Atmosphere and Ocean, University of Washington, Seattle, Washington, USA; ^eUniversity of Florence, Sesto Fiorentino, Florence, Italy

Q1

ABSTRACT

10 *In situ* atmospheric aerosol measurements have been performed from a Manta unmanned aircraft system (UAS) using recently developed miniaturized aerosol instruments. Flights were conducted up to an altitude of 3000 m (AMSL) during spring 2015 in Ny-Ålesund, Svalbard, Norway. We use these flights to demonstrate a practical set of miniaturized instruments that can be deployed onboard small UASs and can provide valuable information on ambient aerosol. Measured properties include size-resolved particle number concentrations, aerosol absorption coefficient, relative humidity, and direct sun intensity. From these parameters, it is possible to derive a comprehensive set of aerosol optical properties: aerosol optical depth, single scattering albedo, and asymmetry parameter. The combination of instruments also allows us to determine the aerosol hygroscopicity.

ARTICLE HISTORY

Received 1 October 2016
Accepted 29 January 2017

EDITOR

Jian Wang

1. Introduction

15 Aerosols have been singled out as the atmospheric component with the largest uncertainties regarding its direct and indirect effect on the earth radiative budget (Boucher et al. 2013). Large efforts have been undertaken to assess these effects on a global scale by measuring aerosol burdens using space-based as well as ground-based remote sensing (Li et al. 2009; Kremser et al. 2016). While data products and modeling techniques have continuously been improved (Levy et al. 2013; Xu and Wang 2015), limited information on vertical variability and physical properties hamper the progress toward a more precise evaluation of aerosol direct and indirect radiative effects.

20 Vertically resolved *in situ* aerosol properties are commonly studied in aircraft campaigns. While providing very detailed measurements of aerosol properties, these campaigns are very costly and for that reason are limited temporally and spatially. Aerosols in the troposphere have lifetimes of days to weeks. Understanding their evolution requires extensive observations because aerosols spread far from their sources yet never become well-mixed enough for a few observations to characterize a global distribution of pollutants. Furthermore, aerosols

continuously change both chemically and physically during their lifetimes. Frequent and globally distributed vertical profiles rather than ground-based measurements alone are highly desired in order to understand the processes that control aerosols and their subsequent effects on air quality and climate.

25 Recent progress in the development of small size unmanned aircraft systems (UAS) has created alternative platforms for atmospheric measurements. With the prospect of conducting *in situ* aerosol measurements at a fraction of the cost of that needed for traditional air campaigns, various research groups are focusing on the development of miniaturized instruments in order to match the tight restrictions on volume, mass, and power consumption (Ramana et al. 2007; Corrigan et al. 2008; Bates et al. 2013; de Boer et al. 2016; Murphy et al. 2016; Gao et al. 2016). These restrictions furthermore put a value on a minimal set of aerosol instruments that can collect a comprehensive set of aerosol properties at adequate accuracies. Based on these new instrument developments, Gao et al. (2015) have proposed a Global Ozone and Aerosol profiles and Aerosol Hygroscopic Effect and Absorption optical Depth (GOA²-HEAD) network, which will use a fleet of small UASs

equipped with different instrument packages for atmospheric profiling.

In this article, we present atmospheric measurements of *in situ* dry aerosol particle size distributions for diameters between 150 and 2500 nm, *in situ* aerosol absorption, and changes in sun radiance with altitude onboard a Manta UAS. These measurements were made using an instrument package that in combination with ozone measurements is suitable for the GOA²HEAD network. We demonstrate how this particular ensemble of instruments can be used to bound the aerosol hygroscopicity values, a property with particularly large effects on optical properties of atmospheric aerosols (Haywood et al. 1997; Twohy et al. 2009; Brock et al. 2015).

2. Methods

All measurements were conducted in spring of 2015 outside the research village of Ny-Ålesund, Svalbard, Norway. A Manta UAS was used as a platform for an aerosol instrument package that contains five instruments: a condensation nuclei counter, a chemical filter sampler, an aerosol absorption photometer, an optical particle spectrometer, and a sun photometer. Data from the latter three instruments are used in this work. Here, we give a brief introduction to the instruments and theoretical methods relevant to the present study.

2.1. Manta UAV

The Manta is a fixed-wing, gasoline-fueled, medium-duration aircraft. It has a cruise speed of $\approx 26 \text{ m} \cdot \text{s}^{-1}$, a total endurance of up to 4.5 h, and can operate in altitudes of up to 3660 m (Bates et al. 2013). A Cloud Cap (Piccolo) autopilot navigates the aircraft between geographic waypoints and performs the landing on the runway.

2.2. Printed optical particle spectrometer (POPS)

Dry aerosol particle size distributions with optical diameters between 150 and 2500 nm were measured using a Printed Optical Particle Spectrometer (POPS) (in more recent models the detection range improved to 140–3000 nm). POPS detects and sizes particles on the single particle level utilizing the dependence of the scattering intensity on the particles size. It uses a 405 nm laser diode as a light source and collects light with scattering angles between 38° and 142° (Gao et al. 2016). Instrument calibration was performed in a lab environment prior to the campaign with dioctyl sebacate (DOS) aerosols that were size selected with a differential mobility analyzer. In the field, we verified calibrations by conducting single point calibrations using 510 nm diameter

polystyrene latex spheres. During all flights the sampling flow rate was regulated to $3 \text{ cc} \cdot \text{s}^{-1}$ at payload bay pressure and temperature, which for the data analysis was reduced to ambient conditions by multiplying with the ratio between absolute temperatures inside and outside the payload bay. Drying of the sampled aerosols was a byproduct of the strong difference between ambient and payload bay temperatures of 20°C . Therefore, RH values of the sample air inside the POPS instrument never exceeded 24%. For RH values no higher than 24% and a residence time of 0.3 s the majority of aerosol particles likely shrunk to sizes that are smaller than their equilibrium size at RH values of 40% (Kerminen 1997; Chuang 2003).

2.3. Three-wavelength absorption photometer (BMI ABS)

Dry aerosol absorption is measured at three wavelengths, 450, 525, and 624 nm, using a filter-based absorption photometer. The instrument has two filters, a sampling and a reference filter, which were both replaced prior to each flight (Bates et al. 2013). Reported absorption coefficients are reduced to ambient conditions and RH values in the instrument were below 24% (see above).

2.4. Miniature scanning aerosol sun photometer (miniSASP)

Sun and sky radiance were measured at four different wavelength, 460.3, 550.4, 671.2, and 860.7, using a miniSASP (Murphy et al. 2016). To record sun intensity and sky brightness, the photometer performs a continuous almucantar scan, during which the telescope scaffold rotates around the vertical axis while the telescopes are pointing at the elevation of the sun. While scanning with a revolution time of $\approx 30 \text{ s}$, the elevation angle is continuously corrected for the tilt of the underlying platform, here the Manta UAS.

2.5. Temperature and relative humidity measurements

The Manta is equipped with a HC2 temperature and relative humidity (RH) probe from Rotronic Instrument Corporation. Reported values have accuracies of $\pm 0.1^\circ\text{C}$ and $\pm 0.8\%$, respectively.

2.6. Mie theory

We calculate aerosol optical properties from size distributions using Mie theory as described in Bohren and Huffman (1983). Input parameters for these calculations are particle diameter, refractive index of the material the

particle is composed of, and wavelength of the scattered light. For optical properties derived from size distributions measured with POPS, the diameter is the center of the particular diameter bin, the refractive index is that of the calibration material ($n_{\text{DOS}} = 1.455$), and the wavelength is, unless stated differently, that of the green channel of miniSASP (550.4 nm). When hygroscopic growth is applied to a size distribution, the refractive index is adjusted to the particles' water content using a volume-mixing rule, where we use 1.33 for the refractive index of water. In all calculations, the imaginary part of the refractive index is set to zero consistent with very low observed absorption coefficients (see below).

3. Results and discussion

We performed a total of nine flights between April the 19th and May 1st over the fjord Kongsfjorden. In the following, we will discuss in detail one of two flights where conditions (clear sky) and performance (miniSASP was irrecoverably damaged on the fourth flight) enabled us to record data with all three instruments, miniSASP, POPS, and BMI ABS. We recorded vertical profiles between 50 and 3000 m by following a spiral flight pattern with a radius of 1 km and a climbing rate of $0.5 \text{ m} \cdot \text{s}^{-1}$ (Figure 1).

Figure 2a shows a vertical profile with a 30 m resolution of the number size distribution (left) and the total particle concentration (right) as recorded by POPS. In addition, we show on the left the center position of a normal distribution fit to each size distribution in the vertical profile (magenta line).

Aerosol number size distributions are important when assessing numbers of potential cloud condensation nuclei (CCN) and their effect on cloud properties. As illustrated by the magenta line in Figure 2a, the center of the accumulation mode, when present, is well inside of the detection range and the total number of particles inside the accumulation mode can be obtained from fitting a normal distribution to the size distribution.

In addition, it is possible to derive aerosol optical properties from particle size distributions, including the scattering coefficient, asymmetry parameter, and Angstrom exponent, using Mie theory. Due to the nonlinear dependence of optical properties on the particle size, a detailed assessment of potential errors and biases is important.

The presence of a coarse mode with particles outside POPS's sizing range—diameters larger than 2500 nm—can have a significant contribution to aerosol optical properties. Figure 3a shows the average size distribution between an altitude of 0 and 500 m measured by POPS during the same flight discussed above. In addition, we show a size distribution recorded with an aerodynamic particle sizer (APS) during the same period of time and which was located in the Gruvebadet station just outside of Ny-Ålesund. The size distribution recorded by the APS shows no distinct coarse mode, however, number concentrations beyond diameters of 2500 nm are not negligible and will result in a bias in derived optical properties. In Figure 3b, we show the calculated bin-wise scattering coefficients for both instruments. To estimate an upper limit for the scattering from the APS size distribution, we assume large particles to consist of sea salt and therefore use a refractive index of 1.53 (Ebert et al. 2002; Weinbruch et al. 2012). The ratio between scattering from particles larger than 2500 nm and the overall scattering coefficient from 150 to 10,000 nm is 6%. Another potential origin for errors is particles smaller than the lower detection limit of POPS. The small diameter end of the calculated bin-wise scattering coefficient in Figure 3b illustrates the negligible contribution of particles smaller than 150 nm to the overall scattering. This is due to the strong dependence of the scattering cross-section on the particle diameter, which is particularly pronounced for particles in the Rayleigh regime (here $d \lesssim \lambda/\pi = 175 \text{ nm}$). A well-known error source in experiments and simulations that are based on light scattering is the uncertainty of the index of refraction of

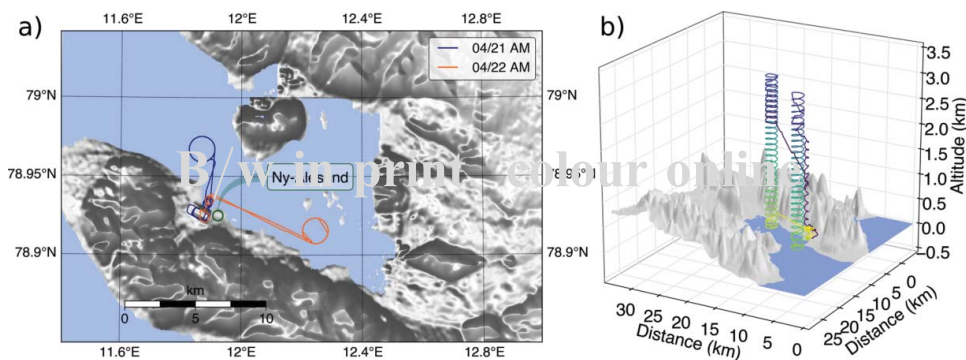


Figure 1. Topview (a) and 3d view (b) of flight paths plotted on a map of Kongsfjorden and the surrounding terrain. Elevation data are taken from ASTER GDEM (ASTER GDEM is a product of METI and NASA).

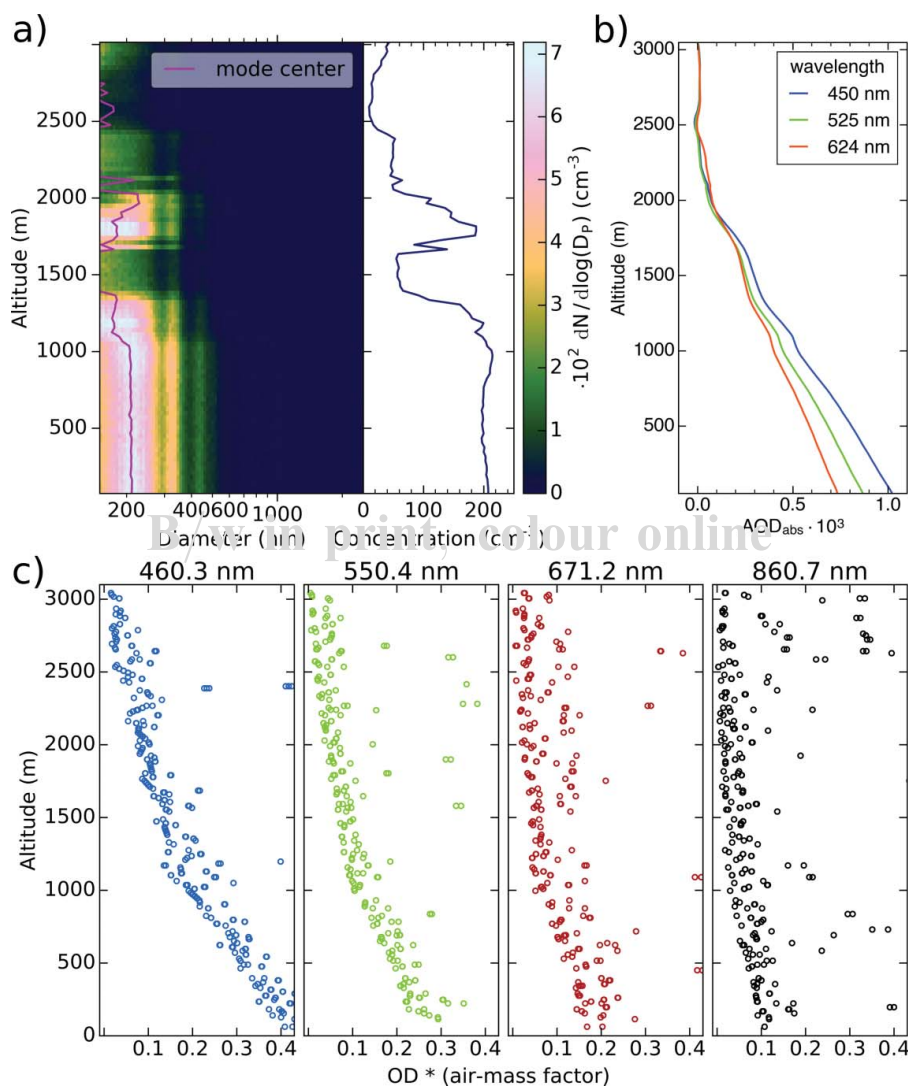


Figure 2. (a)(left) Vertical profile of particle size distributions and (right) particle concentration derived from size distributions recorded by POPS. (b) Accumulated AOD_{abs} from the top of the flight pass for the three wavelengths measured by BMI ABS. (c) Accumulated OD · AMF from the top of the flight path measured by miniSASP. Each plot shows results for one of the four wavelength channels.

ambient aerosol particles (Kassianov et al. 2015). For
 230 optical particle spectrometers with large collection
 angles, like POPS, it can be shown that using the index
 of refraction of the calibration material, here 1.455, in
 the calculations of the scattering coefficient will lead to a
 high bias of up to 15%, assuming the actual index of
 235 refraction is larger than 1.455 but no larger than 1.53.
 Note, this error includes the sizing uncertainty that
 results from the refractive index mismatch between aerosol
 particles and calibration material. We furthermore
 consider a low bias of 10% to calculated scattering coefficients
 240 due to sampling losses particularly of large particles
 that we estimated based on particle loss mechanisms
 described in Baron and Willeke (2011). Including the
 precision of the POPS instrument, we estimate the accuracy
 of scattering coefficients that are derived from size
 245 distribution to be -17% and $+14\%$.

We assume that the sampled aerosol contains spherical
 particles with a uniform refractive index throughout the
 particle and the refractive index to be wavelength independent.
 Further uncertainties will occur if these assumptions are not valid.

Figure 2b shows absorption aerosol optical depth
 AOD_{abs} accumulated from the top of the flight path ceiling
 measured by BMI ABS. Changes in AOD_{abs} are associated
 with elevated absorption coefficients and are clearly
 250 correlated with elevated particle concentrations (right of
 Figure 2a). Therefore, AOD_{abs} stays close to zero in the
 top 1000 m where particle concentrations are very low and
 only increases when particle numbers are sufficiently high.
 Detection limit and uncertainties of the absorption coefficient
 measured by the BMI ABS 255
 have previously been estimated to 0.2 Mm^{-1} and $\pm 33\%$
 (Bates et al. 2013). Here, we applied an additional
 260

250

255

260

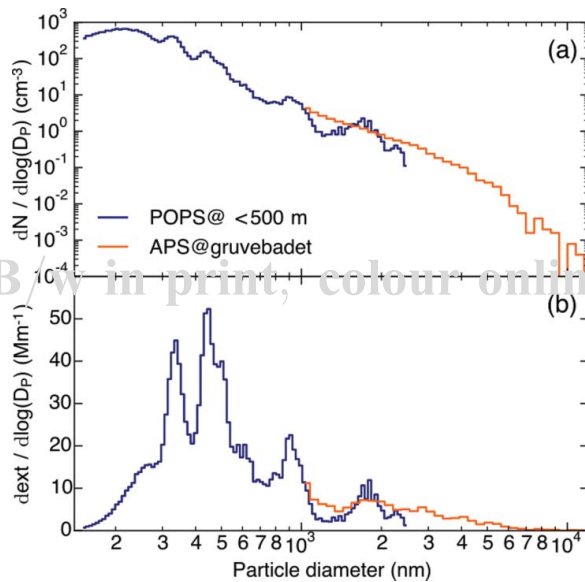


Figure 3. Illustration of the absence of a coarse mode and the limited contribution of particles outside POPS's detection range to the overall scattering coefficient. (a) Size distributions collected by POPS during flight (blue) and an APS instrument located in the Gruvebadet ground station (orange). (b) Bin-wise scattering coefficients of the two size distributions at a wavelength of 550 nm. Note, narrow features in (a) and (b) are artifacts intrinsic to optical sizing techniques. They are particularly pronounced in POPS measurements due to the short laser wavelength. See Gao et al. (2016) for details.

correction to account for the scattering of particles deposited on the filter, which leads to an improved
 265 uncertainty of $\pm 28\%$. Our results show that AOD_{abs} as low as 3×10^{-4} can be resolved.

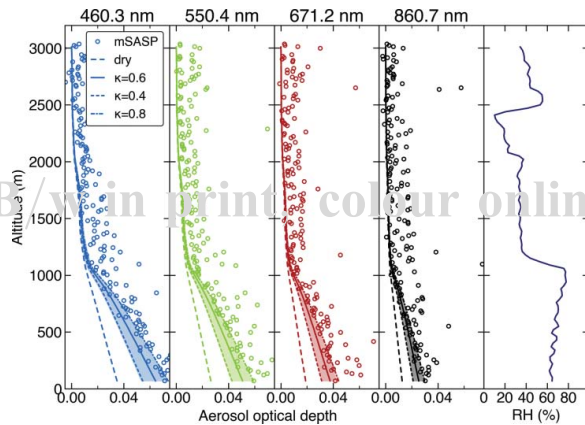


Figure 4. Comparison of vertical profiles of AOD measured by miniSASP (symbols) and derived from size distributions measured by POPS (lines). Subplots are results for the different wavelength channels with the wavelength given in the title and the relative humidity. We assumed different hygroscopicities for the size distribution-derived AOD values, none/dry (dashes), $\kappa = 0.6$ (solid), $\kappa = 0.4$ (dots), and $\kappa = 0.8$ (dash-dotted). Shaded areas mark the uncertainty interval for the size distribution-derived AOD values in case of $\kappa = 0.6$.

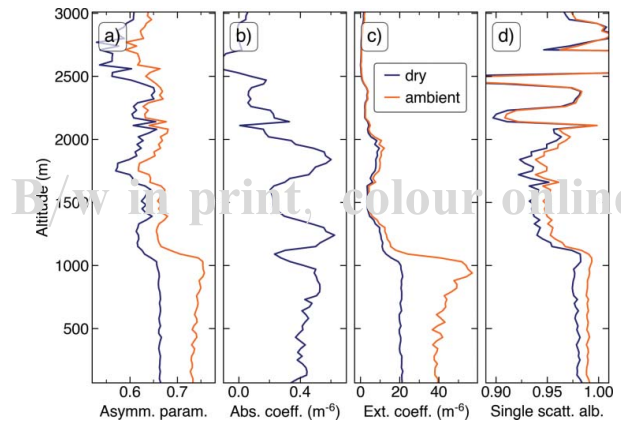


Figure 5. Vertical profiles of further aerosol properties that can be derived from measured datasets, (a) asymmetry parameter, (b) absorption coefficient, (c) extinction coefficient, and (d) single scattering albedo. Blue and orange lines are for dry and ambient conditions, respectively, where the latter was considered by applying hygroscopic growth according to ambient RH and $\kappa = 0.6$.

Within each revolution of miniSASP's telescopes, one distinct peak is recorded in each of the channels with its maximum representing the intensity of the direct sun light I , which can be described by

$$I = I_0 \cdot e^{-OD \cdot AMF}, \quad [1]$$

where I_0 is the unattenuated intensity of the sun light at a given wavelength, OD is the optical depth of the atmosphere (the combination of light scatterings by atmospheric gases and aerosol particles), and AMF is the air mass factor (the ratio of the slant column to the vertical column). **Figure 2c** shows a vertical profile of the logarithm of I , which is proportional to $OD \cdot AMF$.

We furthermore offset values in each channel so that $OD \cdot AMF$ is approximately zero at the ceiling of the flight path. Data in the figure are therefore representing $OD \cdot AMF$

of the atmospheric layer from the top of the vertical profile to the given altitude. Note that the changes in OD between two altitude levels as measured by miniSASP are absolute even though the miniSASP was not calibrated absolutely. Data for all four wavelengths shown in **Figure 2c** appear to be significantly noisier than data collected when the instrument is on a fixed platform (Murphy et al. 2016). We attribute the noise to insufficient attitude compensation during flight, in particular during rapid changes of the plane's roll, which changed up to 15° at frequencies larger than 0.5 Hz. Assuming all short-term variations in the peak intensities to be due to incomplete sun transitions an envelope that connects only the smallest $OD \cdot AMF$ values in **Figure 2c** describes the actual behavior of the direct sun intensity. Starting at

285

290

295

the top of each profile $OD \cdot AMF$ increases approximately

linearly with decreasing altitude until about 1100 m. Below 1100 m OD·AMF increases more drastically. Apparent from Figure 2a, this altitude marks the beginning of higher particle concentrations, which results in an increased contribution of AOD to the overall OD. Note that an elevated aerosol layer at ≈ 1800 m has, despite its significant particle load, almost no impact on OD·AMF. In part, this is related to a smaller diameter of the accumulation mode center, which is indicated by the magenta line in Figure 2 and reflected in a reduced asymmetry parameter of the elevated layer as shown in Figure 5a. In addition, particles in the elevated layer are less affected by hygroscopic growth as discussed in more detail below. A comparison of the four wavelengths channels (four plots in Figure 2c) reveals an overall increase in OD·AMF with decreasing wavelength. This finding is consistent with the wavelength dependence of scattering cross-sections of non-absorbing molecules and particles.

In the previous paragraphs, we discussed aerosol properties that are obtained by each instrument independently. However, the unique combination of instruments allows us to derive more properties.

One of these properties is the hygroscopicity of aerosol particles, which is typically measured by running a dried and a humidified aerosol sample through two separate instruments, a practice that is unpractical for UAS deployments. In order to estimate the aerosol hygroscopicity, we derive from recorded size distributions and sun intensities the accumulated aerosol optical depth from the top of the flight path as a function of altitude. The scattering coefficient is calculated from each size distributions at the four miniSASP wavelengths using Mie theory. Accumulated AOD is obtained by integrating over the scattering coefficient from the flight path ceiling to the particular altitude and adding AOD_{abs} as recorded by the BMI ABS. Due to the small contribution from AOD_{abs} ($\approx 2\%$), we refer to this AOD as POPS derived. From sun intensities, we can retrieve AOD by subtracting the contribution of Rayleigh scattering (Bucholtz 1995) from the OD·AMF data and normalizing to the air mass factor, which we simplify to $\sin^{-1}(\gamma)$, where γ is the solar elevation angle.

Figure 4 shows the resulting accumulated AOD, with miniSASP and POPS derived data given by symbols and lines, respectively. AOD values based on the as-measured size distributions are given by dashed lines. Although, the dashed lines follow the general trend of the ambient AOD, they underestimate those by a factor of about two. This deviation can mainly be contributed to the hygroscopic growth of aerosol particles. The large difference between ambient and payload bay temperatures ensures that air sampled by POPS stays below 24% relative

humidity at all times during the flight. Therefore, AOD in Figure 4 that is related to the as-measured size distributions is labeled as dry. Having measured dried and humidified (ambient) aerosol properties allows us to estimate the hygroscopic growth thus the hygroscopicity of the aerosol particles. As discussed above the scattering from aerosols is dominated by particles larger than 150 nm. This allows us to use an expression for the growth factor $d_{\text{RH}}/d_{\text{dry}}$ that is independent of the particle diameter (Rissler et al. 2006),

$$\text{gf} = \sqrt[3]{1 + \kappa \cdot \frac{\text{RH}}{100 - \text{RH}}} \quad , \quad [2]$$

where κ is a measure for the particles hygroscopicity and which can vary between the two extremes 0 and 1.4 for particular organic and pure sodium chloride particles, respectively. Based on κ -Köhler approximation, we calculate growth factors according to ambient relative humidity values (right most plot in Figure 4) and three different κ values, $\kappa = 0.4$, $\kappa = 0.6$, and $\kappa = 0.8$ (Petters and Kreidenweis 2007). Applying the resulting growth factors to the respective size distributions results in AODs given by the solid ($\kappa = 0.6$), dotted ($\kappa = 0.4$), and dash-dotted lines ($\kappa = 0.8$) in Figure 4. The best agreement between the two instruments is achieved when assuming a κ value of 0.6, which agrees well with typical values measured at the Zeppelin station (Silvergren et al. 2014). Results for the other two κ values illustrate the sensitivity of AOD on κ . Apparently, a variation of κ by 30% causes the calculated AOD to vary about $\approx 15\%$ (shaded area in Figure 4). In the described retrieval of the κ value, we applied a single growth factor to each size distributions, which assumes internally mixed aerosols. In case of externally mixed aerosols, the result would be an effective kappa value with limited meaningfulness in particular with respect to cloud condensation nuclei activity. It has been shown that arctic haze measured at Ny-Ålesund is predominantly internally mixed (Covert and Heintzenberg 1993; Engvall et al. 2009). In our approach, we furthermore applied only one κ value to the entire vertical column. In Figure 2a, we clearly see different aerosol layers and it is possible that hygroscopicity varies between layers (Brock et al. 2011) and one could consider applying different κ values to different layers. Figure 4 suggests that only when ambient RH is sufficiently high and the difference between ambient and calculated AODs is large enough, a κ value can be reliably estimated. Here, this is only the case for the boundary layer up to 1000 m where RH reached up to 80%. An elevated aerosol layer at ≈ 1800 m and 40% RH does not result in enough deviation of ambient and dry AOD to make conclusions on its hygroscopicity.

It is important to note that good agreement between the two AOD retrievals is achieved for all wavelength channels without any wavelength-dependent scaling factors. This result gives confidence in the validity of our approach and the absence of significant numbers of large or absorbing particles, which would decrease and increase the wavelength dependence of the AOD, respectively.

In Figure 5, we show further aerosol properties that can be derived from either one dataset or the combined datasets. Considering the result on the aerosols hygroscopicity, we are able to derive those properties not only for dry but for ambient conditions, where we applied hygroscopic growth to the size distribution using ambient RH and $\kappa = 0.6$.

Figure 5a shows the dry and ambient asymmetry parameter g ,

$$g = \frac{1}{2} \int_0^\pi \cos(\theta) \mathcal{P}(\theta) \sin(\theta) d\theta, \quad [3]$$

where θ is the scattering angle and $\mathcal{P}(\theta)$ is the mean scattering phase function as calculated from Mie theory. Larger particles result in more forward scattering, which is associated with an increase in g . Therefore, g is larger for ambient conditions compared to dry conditions, which is particularly pronounced in the more humid boundary layer up to 1000 m.

Figure 5b and c shows the absorption and extinction coefficient, where the prior was measured by the BMI ABS and the latter is the sum of the scattering coefficient calculated from measured particle size distribution and the measured absorption coefficient. These two parameters are the derivative of the accumulated AOD and AOD_{abs} as a function of altitude, which we introduced above. Together with the single scattering albedo ω —the quotient of scattering and extinction coefficient—which is shown in Figure 5d, the absorption and extinction coefficients illustrate variations in aerosol absorption. Note, the enhanced variability of ω above ≈ 2000 m is the result of very low particle concentrations and noise in the absorption measurement.

Above we demonstrate the value of a combined aerosol dataset in an arctic environment. If deployed in a worldwide network as the proposed GOA²HEAD concept, aerosol properties can be very different from those encountered in this study. In the following, we discuss requirements and assumptions that need to be met in order to derive the aerosol properties we introduced above. Several of the presented measurements will be affected by the atmospheric state. A UAS can only be operated under certain weather conditions

depending on the particular model. Retrievals that contain miniSASP data like ambient extinction and aerosol hygroscopicity will only be available in daylight and at sunny conditions or above thick clouds. Size distribution and aerosol absorption measurements by POPS and BMI ABS, respectively, need to be conducted on dry aerosols or at least at a known relative humidity in order to be meaningful. In some UAS configurations, the difference between ambient and payload temperature will not be sufficient to dry aerosols and an additional drying system will be necessary. Aerosol hygroscopicity can only be retrieved when the difference between ambient and dry AODs is large enough, which implies sufficiently high ambient RH and high aerosol loading. Ambient temperature and RH measurements are needed for several calculations. In the present study, we used Mie theory to derive aerosol scattering coefficients and phase functions from particle size distributions. These properties as well as properties that are derived from them, like dry extinction coefficients, dry AOD, single scattering albedo, asymmetry parameters, hygroscopicity, and the correction factor applied to aerosol absorption measurements, will be affected if the Mie theory's assumptions of spherical and homogenous particles is not correct. In this case, it might be necessary to increase uncertainty estimates or replace Mie theory with a more adequate model (Mishchenko et al. 1997). The quality of the hygroscopicity retrieval will furthermore depend on the aerosol mixing state where externally mixed aerosols will provide merely an effective kappa value. Ground-based aerosol measurements that provide additional aerosol properties are of great value to ensure assumptions are correct and narrow uncertainty intervals at least for the boundary layer.

4. Conclusions

In this work, we have presented a set of miniaturized instruments that are capable of producing science-quality data of aerosol physical properties. We show how a unique combination of instruments including an optical particle spectrometer (POPS), a sun photometer (miniSASP), and an absorption photometer (BMI ABS) is capable of providing a valuable set of aerosol parameters necessary to estimate aerosol radiative effects. This includes properties that determine direct radiative effects—vertically resolved ambient extinction, single scattering albedo, and asymmetry parameter—and properties that determine indirect effects—particle concentrations and aerosol hygroscopicity. Our results show that sensitivities of all measurements are sufficient to provide reliable data

for arctic condition and it can be assumed that
500 signal-to-noise levels improve for higher particle concentrations. Note, the retrieval of some aerosol properties will require additional measurements of temperature and relative humidity.

Funding

505 This work was supported by the NOAA Atmospheric Chemistry, Carbon Cycle, Climate, UAS, and Arctic Programs, the NASA Radiation Sciences and Upper Atmosphere Research Programs, and the Gordon and Betty Moore Foundation. The PMEL contribution number is 4573.

510 References

- Baron, P. A., and Willeke, K. (2011). *Aerosol Measurement*, 3rd ed. John Wiley & Sons, Inc., Hoboken, NJ, USA.
- Bates, T. S., Quinn, P. K., Johnson, J. E., Corless, A., Brechtel, F. J., Stalin, S. E., Meinig, C., and Burkhardt, J. F. (2013). Measurements of Atmospheric Aerosol Vertical Distributions above Svalbard, Norway, using Unmanned Aerial Systems (UAS). *Atmos. Meas. Tech.*, 6(8):2115–2120, doi: 10.5194/amt-6-2115-2013.
- 515 Bohren, C. F., and Huffman, D. R. (1983). *Absorption and Scattering of Light by Small Particles*. Wiley, New York.
- 520 Boucher, O., Randall, D., Artaxo, P., Bretherton, C., Feingold, G., Forster, P., Kerminen, V.-M., Kondo, Y., Liao, H., Lohmann, U., Rasch, P., Satheesh, S., Sherwood, S., Stevens, B., and Zhang, X. (2013). Clouds and Aerosols, in *Climate Change 2013: The Physical Science Basis. Contribution of Working Group I to the Fifth Assessment Report of the Intergovernmental Panel on Climate Change*, T. Stocker, D. Qin, G.-K. Plattner, M. Tignor, S. Allen, J. Boschung, A. Nauels, Y. Xia, V. Bex, and P. Midgley, eds., Cambridge University Press, Cambridge, United Kingdom and New York, NY, USA, pp. 571–657.
- 530 Brock, C. A., Cozic, J., Bahreini, R., Froyd, K. D., Middlebrook, A. M., Mccomiskey, A., Brioude, J., Cooper, O. R., Stohl, A., Aikin, K. C., de Gouw, J. A., Fahey, D. W., Ferrare, R. A., Gao, R. S., Gore, W., Holloway, J. S., Hübler, G., Jefferson, A., Lack, D. A., Lance, S., Moore, R. H., Murphy, D. M., Nenes, A., Novelli, P. C., Nowak, J. B., Ogren, J. A., Peischl, J., Pierce, R. B., Pilewskie, P., Quinn, P. K., Ryerson, T. B., Schmidt, K. S., Schwarz, J. P., Sodemann, H., Spackman, J. R., Stark, H., Thomson, D. S., Thornberry, T., Veres, P., Watts, L. A., Warneke, C., and Wollny, A. G. (2011). Characteristics, Sources, and Transport of Aerosols Measured in Spring 2008 During the Aerosol, Radiation, and Cloud Processes Affecting Arctic Climate (ARCPAC) Project. *Atmos. Chem. Phys.*, 11(6):2423–2453, doi: 10.5194/acp-11-2423-2011.
- 545 Brock, C. A., Wagner, N. L., Anderson, B. E., Beyersdorf, A., Campuzano-Jost, P., Day, D. A., Diskin, G. S., Gordon, T. D., Jimenez, J. L., Lack, D. A., Liao, J., Markovic, M., Middlebrook, A. M., Perring, A. E., Richardson, M. S., Schwarz, J. P., Welti, A., Ziemba, L. D., and Murphy, D. M. (2015). Aerosol Optical Properties in the Southeastern United States in Summer – Part 2: Sensitivity of Aerosol Optical Depth to Relative Humidity and Aerosol Parameters. *Atmos. Chem. Phys. Discuss.*, 15(21):31471–31499, doi: 10.5194/acpd-15-31471-2015.
- Bucholtz, A. (1995). Rayleigh-Scattering Calculations for the Terrestrial Atmosphere. *Appl. Opt.*, 34(15):2765–2773, doi: 10.1364/AO.34.002765.
- Chuang, P. Y. (2003). Measurement of the Timescale of Hygroscopic Growth for Atmospheric Aerosols. *J. Geophys. Res.*, 108(D9):1–13, doi: 10.1029/2002JD002757.
- 560 Corrigan, C. E., Roberts, G. C., Ramana, M. V., Kim, D., and Ramanathan, V. (2008). Capturing Vertical Profiles of Aerosols and Black Carbon over the Indian Ocean using Autonomous Unmanned Aerial Vehicles. *Atmos. Chem. Phys.*, 8:737–747, doi: 10.5194/acpd-7-11429-2007.
- Covert, D. S., and Heintzenberg, J. (1993). Size Distributions and Chemical Properties of Aerosol at Ny Ålesund, Svalbard. *Atmos. Environ. Part A Gen. Top.*, 27(17–18):2989–2997, doi: 10.1016/0960-1686(93)90331-R.
- 570 de Boer, G., Palo, S., Argrow, B., LoDolce, G., Mack, J., Gao, R. S., Telg, H., Trussel, C., Fromm, J., Long, C. N., Bland, G., Maslanik, J., Schmid, B., and Hock, T. (2016). The Pilatus Unmanned Aircraft System for Lower Atmospheric Research. *Atmos. Meas. Tech.*, 9(4):1845–1857, doi: 10.5194/amt-9-1845-2016.
- Ebert, M., Weinbruch, S., Rausch, A., Gorzawski, G., Hoffmann, P., Wex, H., and Helas, G. (2002). Complex Refractive Index of Aerosols During LACE 98 as Derived from the Analysis of Individual Particles. *J. Geophys. Res. Atmos.*, 107(21):1–15, doi: 10.1029/2000JD000195.
- Engvall, A. C., Ström, J., Tunved, P., Krejci, R., Schlager, H., and Minikin, A. (2009). The Radiative Effect of an Aged, Internally Mixed Arctic Aerosol Originating from Lower-Latitude Biomass Burning. *Tellus, B: Chem. Phys. Meteorol.*, 61(4):677–684, doi: 10.1111/j.1600-0889.2009.00431.x.
- 585 Gao, R. S., Elkins, J. W., Frost, G. J., Mccomiskey, A. C., Moore, F. L., Murphy, D. M., Ogren, J. A., Petropavlovskikh, I., and Rosenlof, K. H. (2015). *A Novel Approach to Atmospheric Measurements Using Gliding UASs*. Springer International Publishing, Cham, pp. 10–15.
- 590 Gao, R. S., Telg, H., McLaughlin, R. J., Ciciora, S. J., Watts, L. A., Richardson, M. S., Schwarz, J. P., Perring, A. E., Thornberry, T. D., Rollins, A. W., Markovic, M. Z., Bates, T. S., Johnson, J. E., and Fahey, D. W. (2016). A Light-Weight, High-Sensitivity Particle Spectrometer for PM_{2.5} Aerosol Measurements. *Aerosol Sci. Technol.*, 50(1):88–99, doi: 10.1080/02786826.2015.1131809.
- 600 Haywood, J. M., Ramaswamy, V., and Donner, L. J. (1997). A Limited-Area-Model Case Study of the Effects of Sub-Grid Scale Variations in Relative Humidity and Cloud upon the Direct Radiative Forcing of Sulfate Aerosol. *Geophys. Res. Lett.*, 24(2):143–146, doi: 10.1029/96GL03812.
- 605 Kassianov, E., Berg, L. K., Pekour, M., Barnard, J., Chand, D., Flynn, C., Ovchinnikov, M., Sedlacek, A., Schmid, B., Shilling, J., Tomlinson, J., and Fast, J. (2015). Airborne Aerosol in Situ Measurements during TCAP: A Closure Study of Total Scattering. *Atmosphere*, 6(8):1069, doi: 10.3390/atmos6081069. Q2
- 610 Kerminen, V.-M. (1997). The Effects of Particle Chemical Character and Atmospheric Processes on Particle Hygroscopic Properties. *J. Aerosol Sci.*, 28(1):121–132, doi: 10.1016/S0021-8502(96)00069-9.
- 615 Kremser, S., Thomason, L. W., von Hobe, M., Hermann, M., Deshler, T., Timmreck, C., Toohay, M., Stenke, A., Schwarz,

- J. P., Weigel, R., Fueglistaler, S., Prata, F. J., Vernier, J.-P., Schlager, H., Barnes, J. E., Antuña-Marrero, J.-C., Fairlie, D., Palm, M., Mahieu, E., Notholt, J., Rex, M., Bingen, C., Vanhellefont, F., Bourassa, A., Plane, J. M. C., Klocke, D., Carn, S. A., Clarisse, L., Trickl, T., Neely, R., James, A. D., Rieger, L., Wilson, J. C., and Meland, B. (2016). Stratospheric Aerosol-Observations, Processes, and Impact on Climate. *Rev. Geophys.*, 54(2):278–335, doi: 10.1002/2015RG000511.
- 620
- Levy, R. C., Mattoo, S., Munchak, L. A., Remer, L. A., Sayer, A. M., Patadia, F., and Hsu, N. C. (2013). The Collection 6 MODIS Aerosol Products Over Land and Ocean. *Atmos. Meas. Tech.*, 6(11):2989–3034, doi: 10.5194/amt-6-2989-2013.
- 625
- 630
- Li, Z., Zhao, X., Kahn, R., Mishchenko, M., Remer, L., Lee, K. H., Wang, M., Laszlo, I., Nakajima, T., and Maring, H. (2009). Uncertainties in Satellite Remote Sensing of Aerosols and Impact on Monitoring its Long-Term Trend: A Review and Perspective. *Ann. Geophys.*, 27(7):2755–2770, doi: 10.5194/angeo-27-2755-2009.
- 635
- Mishchenko, M. I., Travis, L. D., Kahn, R. A., and West, R. A. (1997). Modeling Phase Functions for Dustlike Tropospheric Aerosols using a Shape Mixture of Randomly Oriented Polydisperse Spheroids. *J. Geophys. Res. Atmos.*, 102 (D14):16831–16847, doi: 10.1029/96JD02110.
- 640
- Murphy, D. M., Telg, H., Eck, T. F., Rodriguez, J., Stalin, S. E., and Bates, T. S. (2016). A Miniature Scanning Sun Photometer for Vertical Profiles and Mobile Platforms. *Aerosol Sci. Technol.*, 50 (1):11–16, doi: 10.1080/02786826.2015.1121200.
- 645
- Petters, M. D., and Kreidenweis, S. M. (2007). A Single Parameter Representation of Hygroscopic Growth and Cloud Condensation Nucleus Activity. *Atmos. Chem. Phys.*, 7 (8):1961–1971, doi: 10.5194/acp-7-1961-2007.
- Ramana, M. V., Ramanathan, V., Kim, D., Roberts, G. C., and Corrigan, C. E. (2007). Albedo, Atmospheric Solar Absorption and Heating Rate Measurements with Stacked UAVs. *Quart. J. Roy. Meteorol. Soc.*, 133(629):1913–1931, doi: 10.1002/qj.172.
- Rissler, J., Vestin, A., Swietlicki, E., Fisch, G., Zhou, J., Artaxo, P., and Andreae, M. O. (2006). Size Distribution and Hygroscopic Properties of Aerosol Particles from Dry-Season Biomass Burning in Amazonia. *Atmos. Chem. Phys. Discuss.*, 5(5):8149–8207, doi: 10.5194/acpd-5-8149-2005.
- Silvergren, S., Wideqvist, U., Ström, J., Sjogren, S., Svenningsson, B. (2014). Hygroscopic Growth and Cloud Forming Potential of Arctic Aerosol Based on Observed Chemical and Physical Characteristics (A 1 Year Study 2007-2008). *J. Geophys. Res. Atmos.*, 119(24):14,080–14,097, doi: 10.1002/2014JD021657.
- 655
- 660
- 665
- Twohy, C. H., Coakley, J. A., and Tahnk, W. R. (2009). Effect of Changes in Relative Humidity on Aerosol Scattering near Clouds. *J. Geophys. Res.*, 114(D5):D05205, doi: 10.1029/2008JD010991.
- Weinbruch, S., Wiesemann, D., Ebert, M., Schütze, K., Kallenborn, R., and Ström, J. (2012). Chemical Composition and Sources of Aerosol Particles at Zeppelin Mountain (Ny Ålesund, Svalbard): An Electron Microscopy Study. *Atmos. Environ.*, 49:142–150, doi: 10.1016/j.atmosenv.2011.12.008.
- Xu, X., and Wang, J. (2015). Retrieval of Aerosol Microphysical Properties from AERONET Photopolarimetric Measurements: 1. Information Content Analysis. *J. Geophys. Res. Atmos.*, 120(14):7059–7078, doi: 10.1002/2015JD023108.
- 670
- 675